BEAM-INDUCED HEATING AND THERMAL ANALYSIS FOR THE EIC HSR CRYOGENIC HELICAL MAGNET AND BPM ASSEMBLY*

M. Sangroula†, M. Anerella, B. Brenton, D. Gassner, K. Hock, C. Liu, F. Micolon, V. Ptitsyn
Brookhaven National Laboratory, Upton, NY, USA

Abstract

The EIC Hadron Storage Ring (HSR) reuses the RHIC yellow ring with substantial reconfiguration. A major challenge is mitigating beam-induced heating of cryogenic components caused by the shorter hadron bunches and an average beam current three times that of RHIC. In addition, large transverse beam offsets at injection due to helical magnet itself generate asymmetric resistive-wall losses in the cryogenic BPM region. To limit these losses, the HSR helical magnet assembly uses a new copper-plated stainless-steel beam pipe with an amorphous-carbon coating. This paper presents heating and thermal analysis of the EIC HSR cryogenic helical magnet and BPM assembly. Thermal simulations show narrow thermal margin for the helical magnet unit, and adequate margin for the BPM assembly.

INTRODUCTION

The Electron-Ion Collider (EIC) [1–4] leverages the existing yellow ring of the Relativistic Heavy Ion Collider (RHIC) as the Hadron Storage Ring (HSR), with substantial upgrades. The HSR accumulates an average beam current of 0.69 A from 290 bunches with a 60 mm rms bunch length in the highest charge-per-bunch scenario, which produces the maximum resistive wall (RW) heating. In addition, the hadron beam undergoes a large horizontal offset of up to ± 20 mm [5] to synchronize bunch collisions with the electron beam. This large radial offset significantly enhances RW heating [6, 7].

In this paper, we investigate beam-induced heating and perform thermal analysis of the HSR cryogenic helical dipole magnet and BPM assembly. Our earlier papers on beam-induced heating and thermal analysis for other EIC components can be found in [8–12]. To perform the thermal analysis, we compute heat loads arising from beam-induced RW losses and electron cloud effects. We then incorporate these heat loads into ANSYS simulations with appropriate boundary conditions to determine the steady state temperature distribution within the helical dipole magnet and BPM assembly.

HSR CRYOGENIC HELICAL MAGNET AND BPM ASSEMBLY GEOMETRY

The HSR helical magnet assembly consists of four superconducting dipole magnet units and a centrally located BPM. All these components reside inside a cryostat (gray tank with a blue helical stripe) as shown in Fig. 1. The total assembly

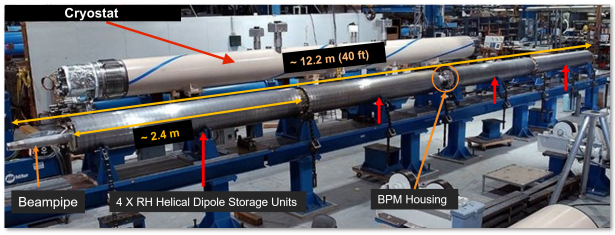

Figure 1: Geometry of the HSR cryogenic helical magnet assembly.

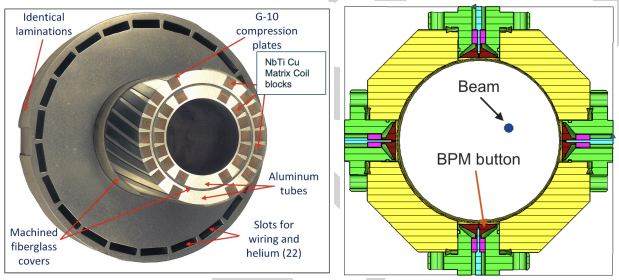

(a) Helical dipole unit (b) Cryogenic BPM

Figure 2: Helical magnet assembly, cross-sectional view.

length is ~12.2 m, with each helical dipole unit measuring ~2.4 m. There are two types of helical dipole magnet assemblies; snakes and rotators. The snakes rotate the spin 180° across all energies and the rotators are used at store energies to rotate the spin into the horizontal plane. The EIC HSR will have total of 6-snakes and 2-rotators [13, 14].

Fig. 2 shows cross-sectional views of the two sections of the helical magnet assembly. The existing RHIC helical dipole, Fig. 2(a), inner beam pipe is made of stainless steel 316L. It also includes two concentric aluminum cylinders of specified thickness that house the helical Nb–Ti coil windings. These aluminum cylinders are externally wrapped with Kelvar and fiberglass (epoxy) to provide electrical insulation and to contain electromagnetic forces from the coil windings [15]. The iron yoke consists of laminated extra-low-carbon steel to enhance magnetic performance. The outer cold mass shell is fabricated from stainless steel 304L.

To adapt the helical dipole for the HSR, we replace the existing (inner) beam pipe with a new stainless steel 316L pipe coated with a 25 μm copper layer, followed by a nanometer-scale (~300-500 nm) amorphous carbon film. The copper layer reduces beam-induced heating, while the amorphous carbon suppresses secondary electron yield (SEY).

Fig. 2(b) depicts the cross-sectional view of the cryogenic BPM showing BPM-buttons and dielectric materials (magenta color). We adopt our original orthogonal button

* Work supported by Brookhaven Science Associates, LLC under Contract No. DE-SC0012704 with the U.S. Department of Energy.
† corresponding author

configuration with the advent of new 90° connectors, which provides ~ 30 % higher beam position sensitivity than earlier *corner-button* configuration. The motivation behind the *corner-button* configuration, reported in Ref. [16], was the vertical space limitation inside the cryostat for connecting cables and feedthroughs. The BPM housing has an inner diameter of 82.80 mm, matching the adjacent beam pipe profile. Each button has a diameter of 18 mm, with a 0.5 mm gap between the button and its housing. The BPM button, BPM housing and button body (button housing) are respectively made of solid copper, internally copper-plated stainless steel, and stainless steel 316L. The feedthrough pin connected to the button is made of inconel 718, and is surrounded by dielectric (SiO_2) to provide the vacuum seal.

Beam-induced heating in the HSR cryogenic helical magnet and BPM assembly arises primarily from resistive wall (RW) losses and electron cloud effect, which we discuss separately in the following sections.

RW HEATING

The largest transverse orbit excursion (dy) in a helical magnet assembly occurs in the snakes at injection, refer to Fig. 3. Additionally, a radial shift (dx) is needed at 100 GeV to match f_{rev}. The proton beam parameters with significant orbit offsets (dx, dy) are listed in Table 1. A comparison of RW losses shows that the 100 GeV store energy case produces the highest heating due to its shorter bunch length, despite having smaller offsets than the injection. As the RW losses are higher in the snakes than rotators, we use the term snake magnet in stead of helical magnet hereafter.

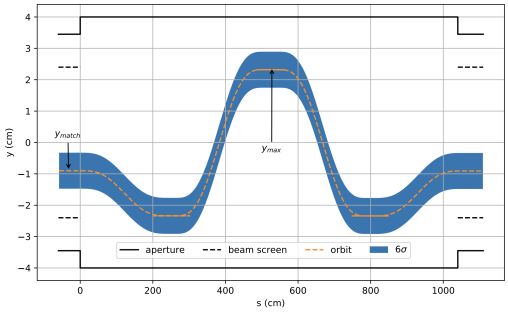

Figure 3: A plot showing the beam offset inside the snake assembly at the injection energy (from Ref. [13]).

Table 1: HSR proton beam parameters in the snake assembly with larger beam offsets (dx, dy).

Beam Energy (GeV)	Beam Offset (mm)	Bunch length (rms, mm)	Bunch charge (nC)	Bunch pattern (NA)
Injection	(0, 23)	500	44	290
100	(12, 6.5)	60	30.5	290

We perform CST simulations for the 100 GeV store energy using the beam parameters listed in Table 1. We evaluate RW losses separately for the snake BPM and the beam pipe. For a worst-case estimate, we include an additional 3 mm radial offset in dx to account for mechanical and injection oscillation tolerances, resulting in total beam offsets of $(dx, dy) = (15, 6.5)$ mm. The resulting losses for individual BPM components are summarized in Table 2.

Table 2: RW Losses on the Snake BPM at 100 GeV

Component	Material	Position	Loss (mW)
Button	Copper	Right	3.75
		Left	0.34
		Top	1.01
		Bottom	0.55
Button Body	Steel 316L	Right	20.19
		Left	2.94
		Top	5.40
		Bottom	4.82
Feedthrough Pin	Inconel 718	Right	12.06
		Left	1.76
		Top	3.21
		Bottom	2.88

The offset beam produces strongly asymmetric RW losses. To capture this, we perform a piece-wise loss analysis by dividing the copper beam pipe into 18 segments, each spanning 20°, as shown in Fig. 4. The segment closest to the beam experiences the highest power deposition.

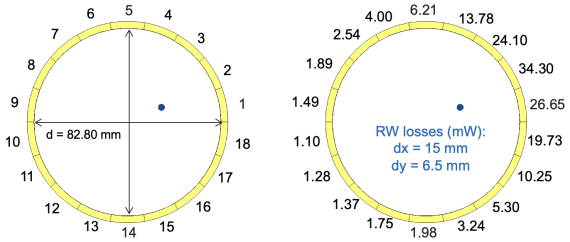

Figure 4: CAD model of the beam pipe slicing into 18-pieces (left). Piece-wise RW loss around the copper pipe of length 200 mm (right) at the 100 GeV store energy.

Anomalous Skin Effect and Magneto Resistance

After evaluating RW losses, we scale them to cryogenic conditions by accounting for the residual resistance ratio (RRR), magnetoresistance (MR) effect, and anomalous skin effect (ASE). The ASE depends on the bunch spectrum (i.e., bunch length) while the MR depends on the magnetic field. Both effects also vary with the RRR value. Detailed formulations of these effects are provided in Refs. [6, 17]. We apply scaling factors for ASE and MR for 60 mm bunch length at the magnetic field of 4 T.

ELECTRON CLOUD HEATING

Electron cloud formation inside the beam pipe introduces an additional heat source if not adequately suppressed. In the snake assembly, electron-cloud heating peaks at the beam pipe center for SEY > 1.25 and decreases with increasing

beam offset, while remaining very small for SEY < 1.2. Detailed calculations are reported in Ref. [18]. To mitigate electron-cloud effects, we apply a nanometer-scale amorphous carbon (aC) coating on the copper layer. The aC layer has a negligible impact on RW heating.

THERMAL ANALYSIS

We performed thermal analysis separately for the snake magnet (helical dipole unit) and the snake BPM by incorporating heat loads from RW losses and electron cloud effect, as mentioned in the earlier sections, into ANSYS simulations. We assumed a conservative SEY value of 1.1 for the beam pipe with amorphous carbon (aC) coating, although properly conditioned coatings may achieve lower values.

An additional heat load in the snake BPM arises from thermal conduction along the instrumentation cable from the 300 K warm end to the cryogenic pickup. To reduce this load, we include two thermal intercepts along the cable at 80 K (heat shield) and 4.65 K (vacuum can enclosure).

For the heat extraction, the snake BPM lies in an enclosure surrounded by 4.65 K helium within the cold mass. For the snake magnet, we circulate liquid helium at the same temperature of 4.65 K via cooling channels. To ensure conservative estimates, we modeled the annular helium channel as static (neglecting convective flow) and used the maximum beam offset however, the maximum offset only occurs at a short section of the magnet unit. Detailed thermal analysis for this whole magnet assembly can be found in Ref. [19].

The simulations predict a maximum temperature of 24.34 K in the snake BPM, located near the central feedthrough pin (Fig. 5(a)). For the helical dipole, the maximum temperature reaches 4.84 K near the inner beam tube and 4.71 K in the superconducting coil (Fig. 5(b)).

We aim to maintain the superconducting coil temperature below 4.75 K based on quench-margin considerations obtained from RHIC operating experience and corresponding thermal analysis. The inner beam pipe can tolerate higher temperatures (up to ~10 K). For the snake BPM, localized regions (e.g., buttons) may reach temperatures up to ~45 K. This limit is guided by vacuum considerations to avoid gas desorption at elevated temperatures, while the BPM structure itself remains robust to bakeout up to 300°C without performance degradation.

Because the snake magnet has a tight thermal margin, we perform a sensitivity study over the copper RRR. The results show that the maximum temperatures of the superconducting coil and beam pipe saturate for RRR values ≥ 50, as shown in Fig. 5(c).

SUMMARY AND FUTURE WORKS

In this paper, we presented beam-induced heating and thermal analysis of the EIC HSR cryogenic snake BPM assembly. The thermal simulations predicted a maximum temperature of 24.34 K in the BPM and 4.71 K in the superconducting coil of the helical dipole for 100 GeV store energy. We will further refine the heating and thermal analysis for this assembly and other EIC components in future work.

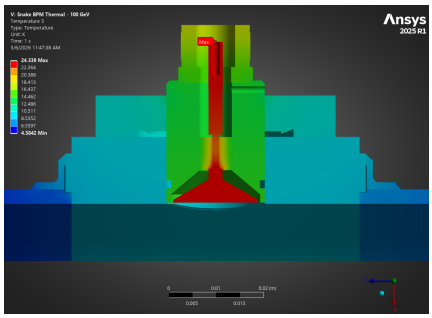

(a)

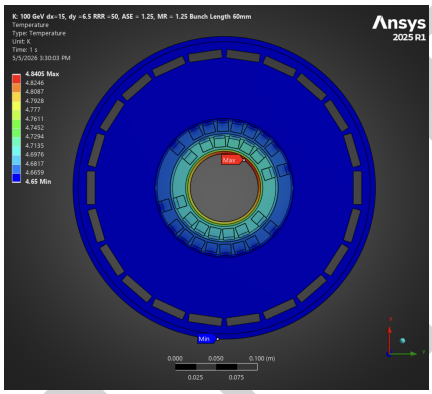

(b)

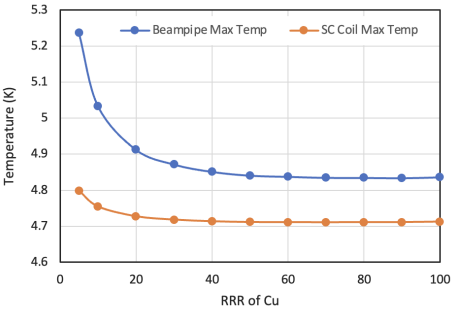

(c)

Figure 5: (a) Thermal distribution showing maximum temperature on the (a) Snake BPM, and (b) Snake magnet. (c) Temperature dependence plot with RRR for the magnet.

ACKNOWLEDGEMENTS

The authors would like to acknowledge S. Verdu-Andres, C. Hetzel, D. Holmes, R. Gupta, J. Tuozzolo, C. Runyan, and S. Nayak for providing invaluable guidance and support for this analysis.

REFERENCES

[1] https://www.bnl.gov/eic/.

[2] C. Montag *et al.*, "Electron-Ion Collider Design Status", in *Proc. IPAC'22*, Bangkok, Thailand, pp. 1954–1957, Jul. 2022. doi:10.18429/JACoW-IPAC2022-WEPOPT044

[3] C. Montag *et al.*, "Design status of the Electron-Ion Collider", in *Proc. IPAC'23*, Venice, Italy, pp. 136–139, Sep. 2023. doi:10.18429/JACoW-IPAC2023-MOPA049

[4] C. Montag *et al.*, "The EIC accelerator: design highlights and project status", in *Proc. IPAC'24*, Nashville, TN, USA, pp. 214–217, Jul. 2024. doi:10.18429/JACoW-IPAC2024-MOPC67

[5] S. Peggs *et al.*, "Large Radial Shifts in the EIC Hadron Storage Ring", in *Proc. IPAC'21*, Campinas, Brazil, May 2021, pp. 1443–1446. doi:10.18429/JACoW-IPAC2021-TUPAB042

[6] S. Verdu-Andres and M. Sangroula, "Beam-induced heat deposited in the EIC HSR screens", Brookhaven National Lab.(BNL), Upton, NY (United States), Rep., 2023.

[7] S. Verdu-Andres, "Beam-impedance consideration for the EIC HSR screen", Brookhaven National Laboratory (BNL), Upton, NY (United States), Rep., 2023.

[8] M. P. Sangroula *et al.*, "Localized Beam Induced Heating Analysis of the EIC Vacuum Chamber Components", in *Proc. NAPAC'22*, Albuquerque, NM, USA, pp. 833–836, Nov. 2022. doi:10.18429/JACoW-NAPAC2022-WEPA85

[9] M. Sangroula *et al.*, "Beam Induced Heating Analysis Update for The EIC Vacuum Chamber Components", Brookhaven National Laboratory (BNL), Upton, NY (United States), Rep., 2023.

[10] F. Micolon, D. Gassner, C. Hetzel, I. Pinayev, M. Sangroula, and S. Verdu Andres, "Thermal simulation of the HSR arc BPM Module for EIC", Brookhaven National Lab.(BNL), Upton, NY (United States), Rep., 2023.

[11] M. Sangroula *et al.*, "Resistive wall heating and thermal analysis of the EIC HSR beam screen", in *Proc. IPAC'24*, Nashville, TN, USA, pp. 759–762, Jul. 2024. doi:10.18429/JACoW-IPAC2024-MOPS22

[12] M. Sangroula *et al.*, "Update on the beam-induced heating and thermal analysis for the EIC vacuum chamber components", in *Proc. IPAC'24*, Nashville, TN, USA, pp. 755–758, Jul. 2024. doi:10.18429/JACoW-IPAC2024-MOPS21

[13] K. Hock and V. Ptitsyn, "Snakes for the hadron storage ring", Brookhaven National Laboratory (BNL), Upton, NY (United States), Rep., 2025.

[14] K. Hock and V. Ptitsyn, "Rotators for the hadron storage ring", Brookhaven National Laboratory (BNL), Upton, NY (United States), Rep., 2026.

[15] E. Willen *et al.*, "A Helical Magnet Design for RHIC", in *Proc. PAC'97*, Vancouver, Canada, May 1997, paper 3P010, pp. 3362–3364.

[16] M. Sangroula *et al.*, "Design of the cryogenic BPM pick-up for the EIC hadron storage ring", in *Proc. IPAC'24*, Nashville, TN, USA, pp. 2199–2202, Jul. 2024. doi:10.18429/JACoW-IPAC2024-WEPG10

[17] S. Verdu Andres and M. Sangroula, "Beam-induced Heat Deposition in the EIC HSR Screen", Brookhaven National Lab.(BNL), Upton, NY (United States), Rep., 2023.

[18] S. Verdu-Andres, "Electron cloud thresholds at the arcs of the Electron-Ion Collider hadron storage ring", Brookhaven National Laboratory (BNL), Upton, NY (United States), Rep., 2023.

[19] B. Brenton *et al.*, "Thermal Analysis of Helical Magnets for Hadron Storage Ring", Brookhaven National Lab.(BNL), Upton, NY (United States), Rep., in preparation.